Response to NRC 2017-2027 Decadal Survey Request for Information #2:

"Linkages of salinity with ocean circulation, water cycle, and climate variability"

Tong Lee (Jet Propulsion Laboratory, California Institute of Technology)
Simon Yueh (Jet Propulsion Laboratory, California Institute of Technology)
Gary Lagerloef (Earth and Space Research)
Mike Steele (University of Washington)
Andrew Thompson (California Institute of Technology)
Mar Flexas (California Institute of Technology)
Arnold Gordon (Columbia University)
Shannon Brown (Jet Propulsion Laboratory, California Institute of Technology)
Tim Liu (Jet Propulsion Laboratory, California Institute of Technology)

Other US co-authors (in last-name alphabetical order):
Eric Bayler (National Oceanic and Atmospheric Administration)
Fred Bingham (University of North Carolina Wilmington)
Subrahmanyam Bulusu (University of South Carolina)
Kyla Drushka (University of Washington)
Paul Durack (Lawrence Livermore National Laboratory)
Seymon Grodsky (University of Maryland)
Ricardo Matano (Oregon State University)
Georgy Manucharayan (California Institute of Technology)
Thomas Meissner (Remote Sensing Systems)
Nadya Vinogradova (Atmospheric and Environmental Research)
Frank Wentz (Remote Sensing Systems)
Lisan Yu (Woods Hole Oceanographic Institution)

Non US co-authors
Georg Heygster (University of Bremen, Germany)
Jacqueline Boutin (University of Paris, France)
Benjamin Rabe (Alfred-Wegener-Institut Helmholtz Center, Germany)
Aida Alvera Azcarate (University of Liège, Belgium)
Christine Gommenginger (National Oceanographic Centre, UK)
Marcos Portabella (Institute of Marine Sciences, Spain)
Nicolas Reul (French Research Inst. for Exploitation of the Sea –IFREMER, France)
Monica Rhein (University of Bremen, German)
Roberto Sabia (Telespazio-Vega UK Ltd. For European Space Agency)
Meric Srokosz (National Oceanographic Centre, UK)
Detlef Stammer (University of Hamburg, Germany)

1. Science and Application target, its importance, and how the understanding in one or more of the Decadal Survey Themes is advanced by addressing it

This white paper addresses the enhancement and continuity of space-based measurements of global sea surface salinity (SSS) to study the linkages of ocean circulation with the water cycle and climate variability, as well as to facilitate biogeochemistry research. Improving sea-ice thickness measurements for studying ocean-cryosphere-water cycle linkages is a secondary goal.

Science and application targets:

(1) To determine the magnitudes of SSS changes in the Arctic Ocean over ice-free regions during summer, the regional dependence (e.g., Eurasian versus North American sectors), and the pathways of Arctic Ocean outflow to the North Atlantic Ocean.

(2) To characterize SSS changes in the high-latitude Southern Ocean, including the meridional gradients across the Antarctic Circumpolar Current (ACC).

(3) To extend NASA's SSS measurements to study the linkages between the ocean and other elements of the water cycle, to constrain the highly uncertain elements (e.g., oceanic evaporation-minus-precipitation (E-P) and continental runoff), and in particular, to reduce the uncertainty of basin-scale E-P estimates to within 3 cm/year.

(4) To constrain global ocean and coupled ocean-atmosphere data assimilation systems used for ocean process studies, initialization of seasonal-to-interannual prediction, short-term ocean forecasts, as well as for driving biogeochemistry models.

Importance of global SSS measurements to Earth System Science research:

As discussed in a community white paper in response to the Decadal Survey initial Request for Information[1], satellite SSS measurements are important in the following areas:

Ocean circulation and climate. SSS plays a more critical role than sea surface temperature (SST) in influencing surface density of high-latitude oceans and thereby affects a large spectrum of high-latitude ocean processes such as advection, mixing, convection, and water-mass formation[2]. Higher (lower) SSS can destabilize (stabilize) the water column, thus influencing the formation of dense water masses and the sequestration of heat and carbon into the deep ocean. These processes have significant implications for the large-scale meridional overturning circulation (MOC) and the related transports of heat, freshwater, and carbon[3], and the spatiotemporal variability of oceanic heat content such as anomalies associated with the so-called "global warming hiatus"[4]. The Arctic Ocean is freshening due to the combined effects of melting sea ice, increased continental runoff, and ocean circulation changes[5]. The interaction of Arctic Ocean outflow waters with the saltier North Atlantic waters has strong implications for the North Atlantic circulation. In the Southern Ocean, the weak vertical stratification accentuates the effectiveness of small salinity changes on ventilation, deep convection, and the MOC[6]. Changes in the distribution of Antarctic sea ice extent and thickness and the associated SSS variations are expected to play a major role in the future evolution of global overturning rates[7]. SSS has significant influence on the Antarctic Intermediate Water and Subantarctic Mode Water, which are fundamental to Southern Ocean air-sea fluxes[8,9]. In the tropics, rain-induced freshening causes formation of the so-called "barrier layer", which inhibits vertical heat exchange between the mixed layer and thermocline and regulates air-sea interaction and related climate variability[10,11] (at high latitudes, ice melt may play a similar role). SSS is also important to understanding and predicting climate variability such as the El Niño-Southern Oscillation[12-17].

Water cycle. The ocean is a key element of the global water cycle with ~85% (77%) of the global evaporation (precipitation) occurring over the ocean[18-21] (Figure 1). Salinity serves as a good indicator of water cycle changes, integrating the effects of various components of the water cycle on the ocean (e.g., evaporation, precipitation, continental runoff, sea ice melt). It also constraints the poorly known elements of the global water cycle such as oceanic E-P and continental runoff, and regulates the feedback to climate variability[22,23]. Historical multi-decadal SSS observations have provided strong evidence for an acceleration of the water cycle (i.e., "salty

gets saltier and fresh gets fresher" associated with "wet gets wetter and dry gets drier")[21,24,25,58]. Multi-decadal, basin-scale changes in upper-ocean salinity are on the order of 0.05 practical salinity unit (psu)/decade[21,26]. This is equivalent to oceanic E-P changes of 3 cm/year, which is far smaller than the discrepancies among existing E-P products[9]. Therefore, long-term changes in oceanic E-P can be more effectively ascertained when using SSS observations as constraints[9,21]. Although satellite SSS measurements are not as accurate as in-situ observations, NASA's Aquarius satellite has demonstrated the ability to detect large-scale (10^ox10^o) non-seasonal SSS variations to better than 0.05 psu equatorward of 65^o latitudes on monthly time scales[28]. In subtropical ocean regions, the evaporation (that dominates over precipitation) provides the predominant source of moisture carried by atmospheric circulation to continents, thereby affecting terrestrial precipitation and soil moisture. SSS variations in subtropical North Atlantic are found to be a better predictor of Sahel rainfall than SST[29,30].

Biogeochemistry. The marine ecosystem and ocean carbon cycle both strongly depend on ocean circulation[31,32], which is in turn strongly regulated by salinity, especially at high latitudes. In particular, the MOCs associated with the North Atlantic and Southern Ocean play important roles in biogeochmical cycles[33-35]. The Southern Ocean is a major sink for the anthropogenic CO_2 (representing almost ½ of the global oceanic sink) and is characterized by strong interannual-decadal variability[36]. SSS influences oceanic vertical mixing and convection and affects nutrient supply, CO_2 distribution in surface waters, air-sea gas exchanges (e.g., CO_2 and O_2), and carbon sequestration. In the tropics, SSS plays an important role in the spatial distribution of biogeochemical parameters in surface waters, either through its influence on ocean circulation or its relation to rainfall[37, 44] and river discharge[38]. Oceanic total alkalinity, an important parameter for carbon cycle and ocean acidification studies, correlates strongly with salinity[39]. Space-based SSS measurements are providing new resources to enhance biogeochemistry research[40-45].

Knowledge and observing system gaps:

High-latitude oceanic processes. Increased precipitation, river runoff, and sea-ice melt are impacting the Arctic Ocean's freshwater and density structure. However, poor in-situ data coverage (particularly in Russian coastal waters and in the seasonal ice zone) limits our knowledge of the changing SSS patterns and the freshwater outflow pathways to deep-water formation sites in the North Atlantic Ocean as well as the associated consequences. The interaction of the fresher Arctic Ocean outflow with the saltier North Atlantic waters and the consequences on the Atlantic MOC and global ocean heat content need to be further understood[5]. In the Southern Ocean, the temporal SSS variability of the Subantarctic Front (SAF) and Polar Front (PF) zones and the related water-mass formation processes are not well documented, especially in terms of variations across different zonal sectors that are expect to affect global overturning rates[46]. Finally, the current generation of climate models has limited skills in representing high-latitude water mass properties due to crude representations of such physical processes as lateral mixing (especially in the marginal ice zone), convection, and entrainment[47]. These limitations impose uncertainties in the modeled response to climate changes.

The changing water cycle. Deciphering climate change effects on terrestrial elements of the water cycle (e.g., total continental runoff and soil moisture) has been complicated by human activities (e.g., dams and agriculture). Land-based precipitation records are spatially too heterogeneous to provide a continental/global view, and are extremely sparse in tropics/mid-latitudes over many continents[48,49]. Many river discharges are poorly known[19,50]. While progress has been made in space-based measurements of oceanic precipitation, there are still considerable differences in tropical precipitation among different products. There exist no direct evaporation measurements on global scale. Oceanic evaporation is typically estimated empirically from measurements of wind speed, air and sea surface temperature, and humidity and is subject to considerable uncertainty. Uncertainties in both P and E estimates cause substantial discrepancies among E-P products[51,52], including regional differences and global budget.

Model representation. The relatively large errors in oceanic E-P estimates, resulting in global net E-P imbalance and regional uncertainties, are a principal cause for biases and drift in ocean models and data assimilation products. The lack of sufficient global SSS measurements to appropriately constrain models has led to the relatively common practice of relaxing model SSS towards a seasonal climatology. Ocean models and assimilation systems typically are also forced by climatological river discharges, including highly uncertainty estimates for many rivers. These two practices limit model skills in representing SSS because they suppress non-seasonal SSS variations and could introduce erroneous sources of freshwater or salinity into the model state[53-55].

In-situ versus space-based observing systems. The existing near-global in-situ salinity observing system is the Argo array of nearly 4000 autonomous profiling floats (Figure 2). The nominal spacing of one float per 3°x3° (with an average 10-day profiling interval) is inadequate to characterize many features and regions of the world oceans (e.g., mesoscale variability, variations under rain bands, boundary currents, marginal seas, coastal and high-latitude oceans). Although Arctic sea ice extent has been declining in all seasons[56], winter sea ice still covers the entire Arctic Ocean, making deployment of standard Argo floats problematic. Under-ice Argo technology is being developed but the future distribution of such floats will remain sparse compared to satellite sampling. Ice Tethered Profilers provide some SSS observations[57], but at a much higher unit cost. Marginal seas and coastal oceans, directly affected by rivers, are important to the connection of the ocean with the terrestrial water cycle. However, Argo float distributions in these regions are sparse or non-existent due to grounding issue and the divergence caused by strong currents. Space-based SSS measurements have advantages in terms of global coverage and finer spatiotemporal sampling, allowing us to fill the aforementioned knowledge gaps.

Given the importance of SSS measurements to fill these knowledge gaps, addressing the aforementioned targets allows advancements related to **Decadal Survey Theme "IV. Climate Variability and Change: Seasonal to Centennial", Theme "I. Global Hydrological Cycles and Water Resources", and Theme "III. Marine and Terrestrial Ecosystems and Natural Resource Management".** In particular, satellite SSS will enable progress in these themes by improving the understanding in the following areas:

- Impacts of the freshening Arctic Ocean on surface density and the consequence on large-scale ocean circulation and associated property transports oceanic heat content variations.
- Effects of SSS variability in the Southern Ocean, especially on subduction, ventilation, water-mass characteristics, and the related sequestration of heat and carbon into the deep ocean.
- Impacts of SSS on vertical mixing in tropical oceans and air-sea interaction associated with climate variability and on air-sea exchanges of heat, momentum, and gases (e.g., CO_2 and O_2).
- Changes in the water cycle and the relationships among its components (e.g., E-P, oceanic moisture supply for terrestrial precipitation, continental runoff, sea-ice melt).
- Relationships of oceanic freshwater/heat contents with the global energy and water cycles.
- Ocean/climate model representations of ocean/climate processes and climate prediction.

2. Utility of the measured geophysical variable(s) to achieving the science and application target.

SSS measurements can be used to address science and application targets (1) and (2) directly without using other geophysical variables. For target (3), SSS serves as a good indicator of the changes in the water cycle for regions and spatiotemporal scales where the effects of E-P and river discharges are more dominant than those due to ocean dynamics[21, 55, 58,59]. The value of satellite SSS observations toward addressing the science and application targets is greatly enhanced with complementary use of other geophysical measurements obtained in the context of integrated observing and Earth System Science, particularly when addressing target (4), which integrates SSS and other measurements into ocean or coupled ocean-atmosphere modeling and assimilation systems[60-63]. SSS and SST measurements together enable quantification of surface density that is important to ocean circulation and biogeochemistry. SSS measurements, estimates

of E-P and ocean surface currents (derived from altimetry and scatterometry), and mixed-layer depths estimated from Argo observations enable studies of SSS budgets and surface freshwater redistribution. Sea ice thickness measurements, used in combination with other measurements (e.g., SSS, sea ice extent, wind, runoff), supports efforts to decipher the cause for the changing SSS and freshwater content of the Arctic Ocean.

3. The key requirements needed for achieving the science and application target.

Addressing the aforementioned science and application targets requires the enhancement of NASA's space-borne capabilities for observing SSS and sea ice thickness. The related key requirements for the coming decade are listed in Tables 1 and 2. Rationales are provided below.

To maximize the synergy of satellite SSS and SST to monitor surface density, it is necessary to monitor SSS at 25-km spatial resolution, which is the resolution of SST measurements made by passive microwave (PMW) radiometers. This resolution is important to studying SSS variations associated with mid- and low-latitude mesoscale features, boundary currents, tropical rain bands, and major river plumes. It is sufficiently small to resolve the 85-km widths of the SAF and PF in the Southern Ocean[64]. It also enables measurements of SSS (thus surface density) closer to the coasts and sea ice edge than before. Such a spatial resolution is several times finer than Aquarius' 100-150 km footprints and finer than the 40-km resolution of NASA's Soil Moisture Active-Passive (SMAP) satellite, and is over an order of magnitude smaller than the effective resolution of the Argo array (hundreds of km or larger).

The temporal sampling requirement is global coverage every 3 days (shorter than Aquarius' 7 days and the same as that for SMAP), which allows monitoring of synoptic and longer variability and is a few times shorter than the nominal 10-day profiling interval of Argo. This 3-day temporal sampling is also important to the monitoring of the rapid growth of 1st-year (FY) sea ice.

The accuracy requirement for SSS is 0.15 psu for SSS anomalies on monthly and 1° scales and 0.1 on 10° scale, averaged over the global ocean. Defining the accuracies for anomalies as opposed to absolute SSS (akin to altimetry-derived sea level anomalies instead of absolute sea level) is more fundamental to studying spatiotemporal changes of the ocean. These accuracy requirements, already achieved by Aquarius V4.0 SSS[28] (also Figure 3), serve as the baseline requirements for a future satellite salinity mission. The beta version of SMAP SSS[65] (employing only radiometer measurements only due to the loss of the radar) also showed encouraging quality, with a 0.2-psu standard deviation from Argo data on 1°, monthly scales (Figure 4). Were radar data available for the correction of surface roughness effect, the quality would be even better. Moreover, the continuing cal/val effort is expected to further improve SMAP SSS accuracy.

The requirement for sea ice thickness measurement is to be able to measure up to 1.5-m thickness, near the maximum thickness of FY ice, which is dominant in the Southern Ocean and has become more prevalent in the Arctic Ocean, with an accuracy of ~25% (based on SMOS experience[66]). Being able to measure sea-ice thickness up to 1.5 m will fill the gap created by minimum thickness limitations (~1 m) using radar-based technologies (e.g. CryoSat).

4. Likelihood and affordability of achieving the required measurement(s) in the decadal timeframe; potential for leveraging complementary measurements.

There are no new technologies required to achieve the spaceborne observations of SSS and sea ice thickness. The required science measurements can be provided by a dual-band (P-/L-band) radiometer instrument augmented by a L-band radar sharing a conical scanning antenna. The conical scanning approach, similar to SMAP, will provide a 1000-km swath width with global coverage in 3 days. The temporal revisit will be daily or more frequent for latitudes >60^{o}. L-band (~1.4 GHz) radiometer SSS measurements have been performed by the European Soil Moisture Ocean Salinity (SMOS) mission since 2009[67], NASA's Aquarius mission (2011-2015)[68], and NASA's ongoing SMAP mission since April 2015[69]. The instrument concept has significant heritage from Aquarius[68] and SMAP[69] on radar/radiometer electronics and deployable mesh

antenna. To achieve the measurement resolution, a 10-m antenna size is needed (compared to SMAP's 6-m antenna), which allows a spatial resolution of 24 km for the L-band radiometer to meet the required 25-km SSS measurement resolution. The 10-m mesh antenna with no new technology is in the same class of 12-m antenna currently being used for NASA-ISRO SAR (NISAR) and ESA Biomass missions. The momentum control of spinning a 10-m lightweight mesh antenna is within the capability of SMAP design.

The SSS retrieval algorithms[70-73] for L-band instruments also has a significant heritage from Aquarius, SMOS and SMAP. The primary instrument making SSS measurements for these missions is the L-band radiometer (allocated for the radio astronomy observations). SMOS contains only the PMW radiometer, while Aquarius included an integrated scatterometer designed to measure ocean backscatter to remove the surface roughness effect on radiometer brightness temperature (T_B) measurement. Aquarius V4.0 SSS has a globally averaged absolute accuracy of 0.17 psu on 150-km and monthly scales[74]. The temporal SSS anomalies have globally averaged accuracies of 0.12-0.16 (0.08-0.09) psu at 1^o (10^o) and monthly scales[28] (Figure 3). The accuracy of non-seasonal anomalies on 10^o scale is better than 0.05 psu[28] (Figure 5), making it possible to constrain large-scale E-P estimates on decadal time scales to within 3 cm/year[9], target (3) above.

L-band SSS accuracy degrades at high latitudes due to reduced sensitivities of T_B to SSS at low SST. To increase high-latitude SSS accuracy to the levels in the tropics (~0.1 psu[28]), the instrument concept includes a P-band (~600 MHz) radiometer, which has three times better sensitivity to SSS than L-band for SST<5^o C (Figure 6). Based on Aquarius and SMAP heritages, the dual-frequency (P-/L-band) radiometer radiometer will be complemented by a L-band radar to provide data for making surface roughness correction.

Sea ice thickness measurements will be made by the L-/P-band PMW radiometer for FY ice in conjunction with ice thickness data from Cryosat/Icesat2 for thicker sea ice. Cryosat has been acquiring freeboard measurements to estimate sea ice thickness. The uncertainty of the snow depth has a large impact on Cryosat/Icesat2 estimates of thinner sea ice thickness. L-band SMOS and SMAP has been used to map the thickness of thin FY ice but is limited to a maximum thickness of ~50 cm[66,75]. The P-band radiometer frequency can detect thickness up to ~ 1.5 m. The dual-band radiometer provides highly complementary ice thickness data to those from Cryosat and Icesat2.

Although L-band SSS measurements have lower accuracies at high latitudes (~ 0.25-0.6 psu) than those in the tropics/subtropics (~0.1 psu)[28], they are still very useful for studying the Arctic Ocean because of its large spatiotemporal SSS variations [76-79] with spatial gradients as large as 10 psu over 200 km and decadal changes of several psu (Figure 7). The much weaker SSS variations in high-latitude Southern Ocean (0.3-0.5 psu[80,81]) is near the accuracy threshold of L-band SSS. However, P-band SSS measurements can provide three times better accuracy than L-band at high-latitude oceans (Figure 6). For the same 10-m antenna, SSS derived from P-band has a lower resolution (56 km) than L-band (24 km). Given the sparseness of *in situ* SSS measurements in the high-latitude oceans, 56-km resolution measurements still have significant values.

The required radar and radiometer technologies with high calibration stability have been tested in space and shown to meet the target accuracy of SSS. The Aquarius and SMAP radars have both achieved a calibration stability of <0.1 dB in space. The Aquarius radiometer had some small calibration drifts in the early part of the mission, but the source of calibration drift has been fully addressed in the SMAP radiometer design, which has resulted in better that 0.1K calibration stability. Moreover, SMAP has shown excellent performance to mitigate/remove Radio Frequency Interference (RFI) impacts for both radar and radiometer measurements. The required space technologies to address the aforementioned science targets are ready for a space implementation in the 2017-2027 timeframe. The envisioned effort will also help establish the capability for continuing improvement for sustained space-based monitoring of SSS.

The measurement concept described here is highly synergistic to those described by three other white papers in response to the Decadal Survey second Request for Information[82-84].

Table 1 Measurement capabilities and requirements for SSS anomaly for two antenna sizes. The 10-m (6-m) antenna size allows resolving scales of the 1st baroclinic radius of deformation (the scales when Earth rotation becomes important and geostrophic theory applies) up to approximately ±45° (35°). The former latitude range encompasses the full extent of mid-latitude western boundary currents that are important to ocean dynamics and air-sea interaction.

	Spatial resolution (10-m antenna)	Spatial resolution (6-m antenna)	Temporal repeat	Accuracy at 1°, monthly	Accuracy at 10°, monthly
L-band 1.4 GHz (global average)	24 km	40 km	3 days	0.15 psu	0.1 psu
P-band 600 MHz (high-latitude average)	56 km	100 km	3 days	0.15 psu	0.1 psu

Table 2 Measurement capabilities and requirements for sea ice thickness.

	Spatial resolution (10-m antenna)	Spatial resolution (6-m antenna)	Temporal repeat	Accuracy (monthly)	Maximum range of detection
P-band 600 MHz	56 km	100 km	3 days	25%	1.5 m

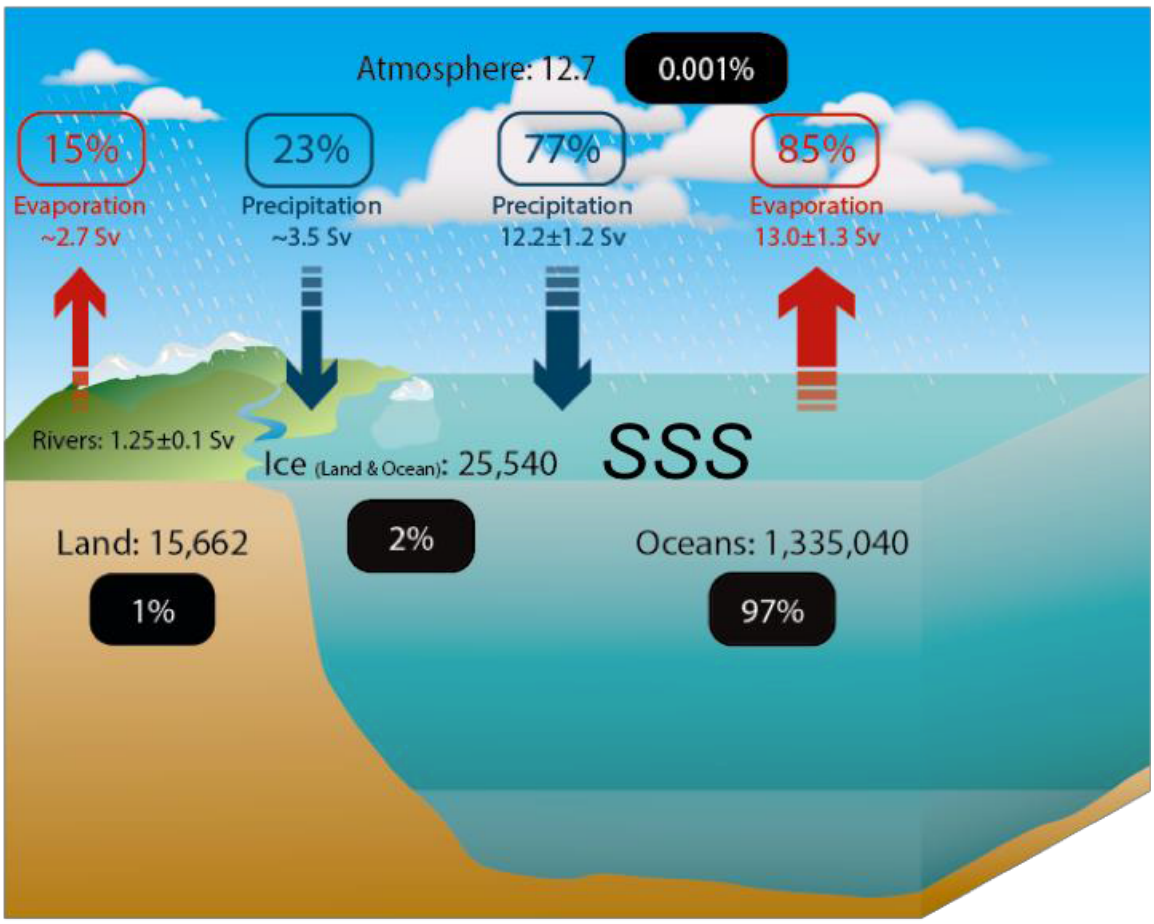

Figure 1. Schematic illustration of key elements of the water cycle. Reservoirs represented by solid boxes (in unit of 10^3 km^3). Fluxes represented by arrows (in unit of 10^6 m^3 /s). Graphics after Durack et al. (2012) with the sources of the estimates obtained from Baumgartner and Reichel (1975), Schmitt (1995), Trenberth et al. (2007), Schanze et al. (2010), and Steffen et al. (2010). SSS links the water cycle with the ocean.

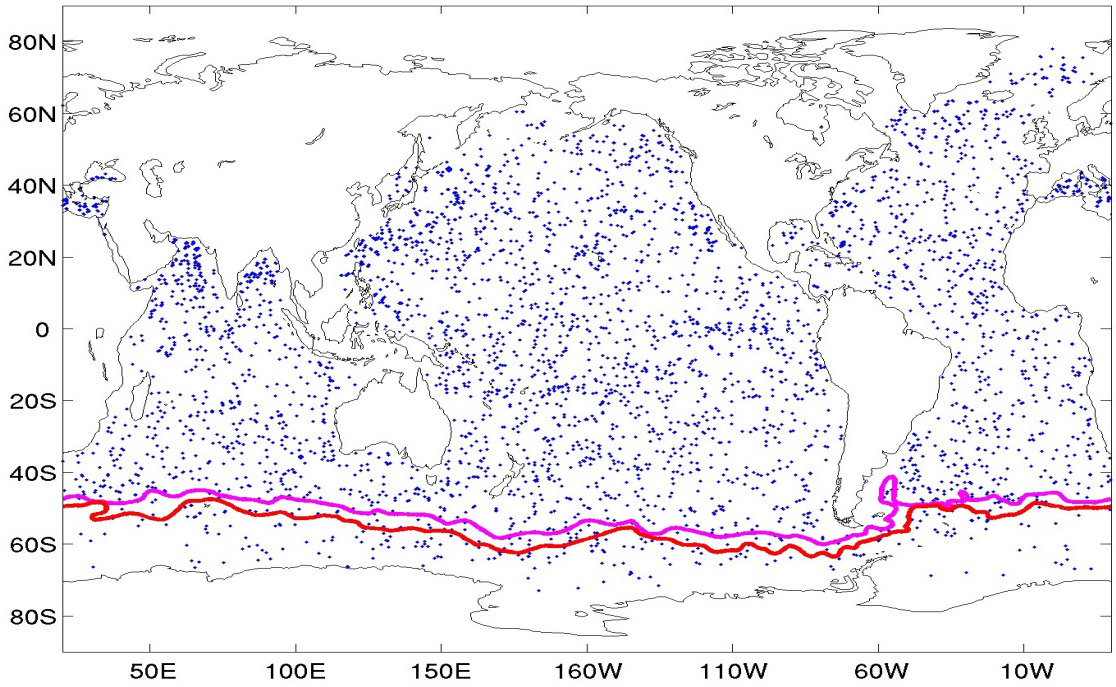

Figure 2. Distribution of Argo floats during a recent 10-day period (1-10 March 2016), with an averaged one float per 3°x3° spacing with a nominal 10-day profiling interval. The magenta and red contours indicate the climatological positions of the Subantarctic and Polar Fronts (SAF and PF) derived from historical hydrographic data (Orsi et al. 1995).

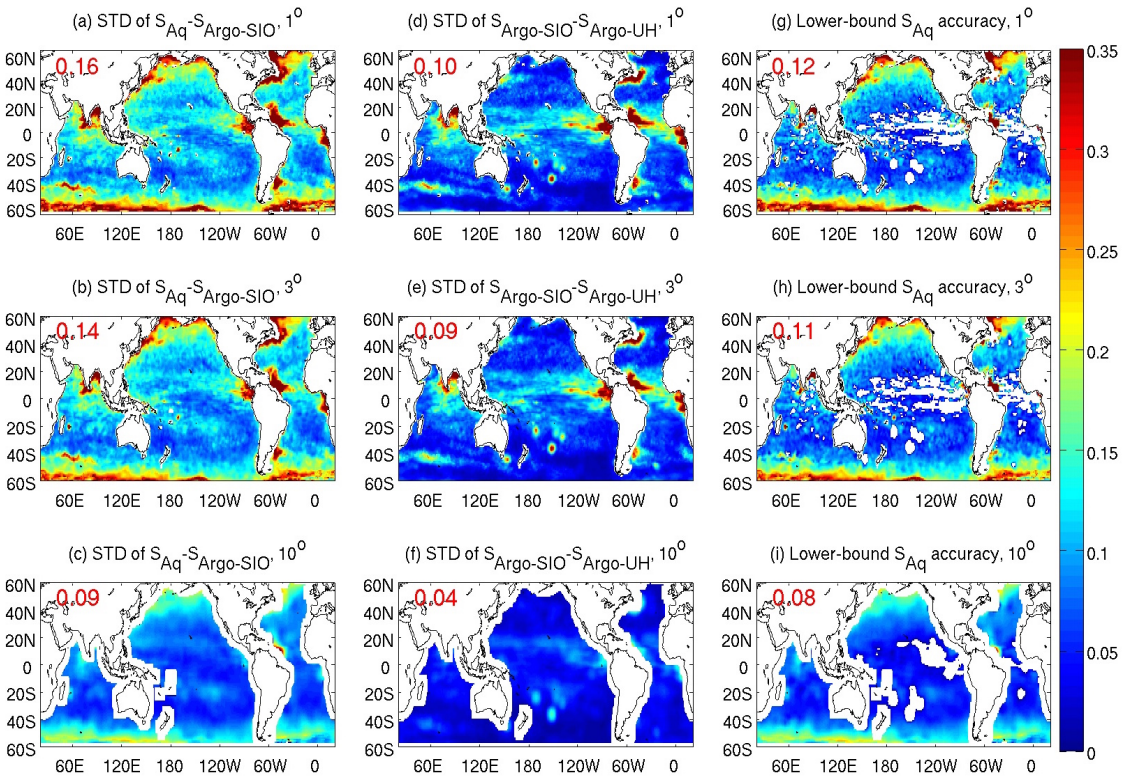

Figure 3. Standard deviation (STD) of SSS differences between monthly gridded Aquarius V4.0 SSS and the 2.5-m Argo OI product from Scripps Institution of Oceanography (Argo-SIO) on 1°x1° (a), 3°x3° (b), and 10°x10° (c) scales. The STD values between two Argo OI products (Argo-SIO and one from the University of Hawaii, Argo-UH) on these three scales are shown in the middle column (d, e, f). The values in the left column represent upper-bound Aquarius SSS accuracies. The right column (g, h, i) are the estimated lower-bound Aquarius SSS accuracies obtained by removing the variance at each location of the middle column from that in the left column then took the square root. The whited-out mid-ocean grid points in (g, h, i) indicate where the discrepancies between the two Argo products are larger than those between the Aquarius and Argo products. The red numbers indicate the respective "global averages" where Argo data are available. After Lee et al. (2016)[28].

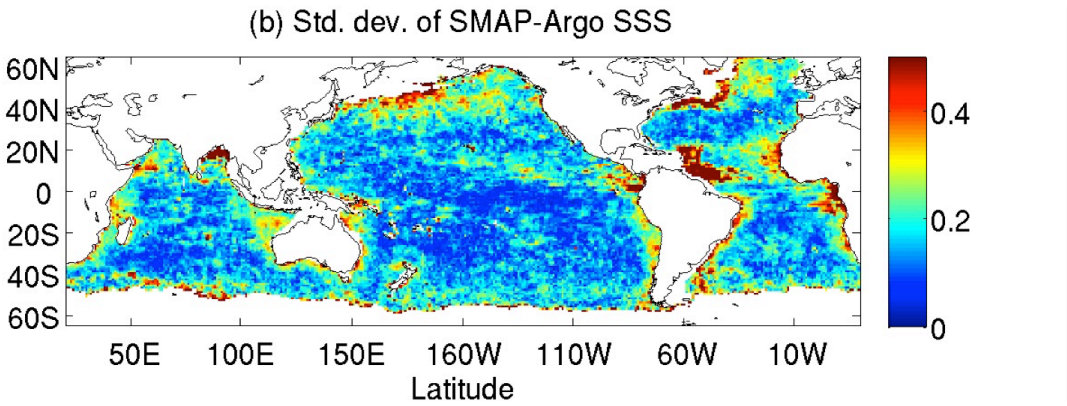

Figure 4. Standard deviation (STD) of the difference between the beta version of SMAP SSS (based on radiometer measurements) with Argo-SIO during May-December 2015. The globally averaged STD value is 0.2 psu.

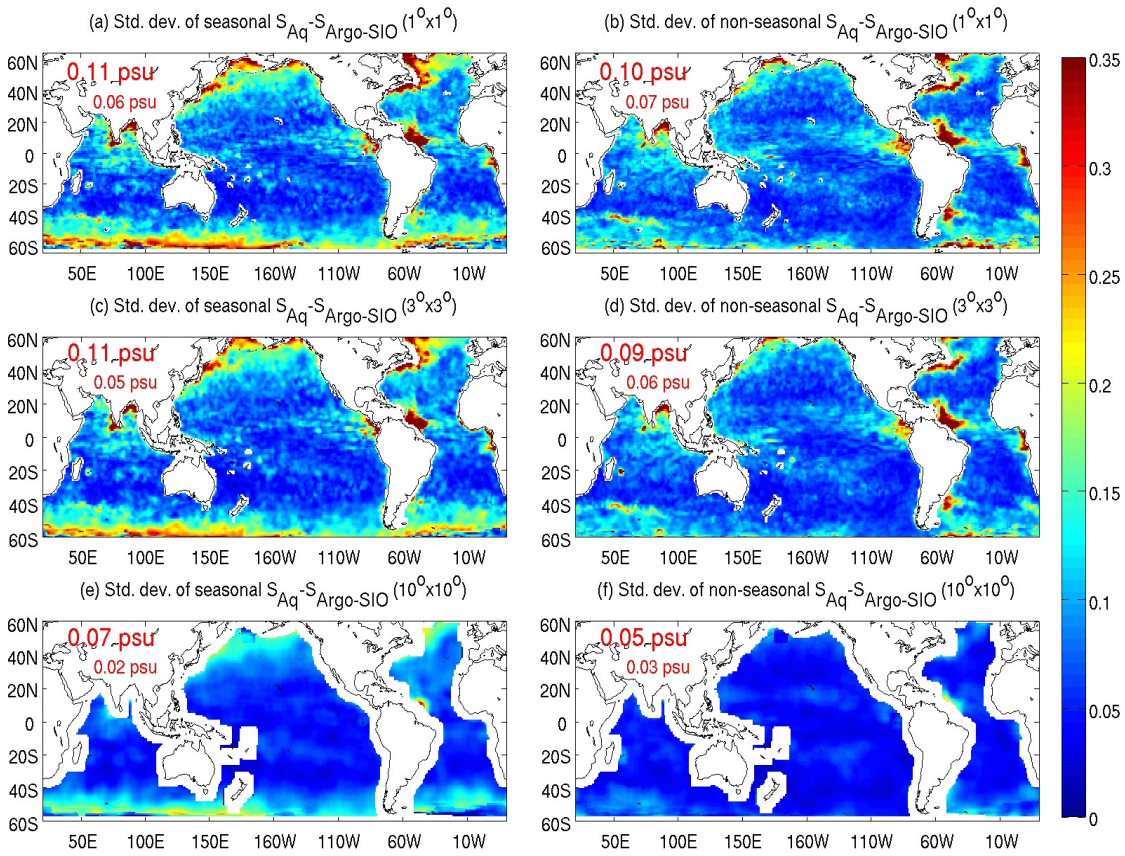

Figure 5. Standard deviation (STD) of seasonal (left) and non-seasonal (right) SSS differences between Aquarius and Argo-SIO on 1°x1° (a, b), 3°x3° (c, d), and 10°x10° (e, f) scales. The red numbers with a larger font are the respective global averages. The red numbers with a smaller font are the corresponding global averages for the standard deviation of Argo-SIO vs Argo-UH seasonal and non-seasonal SSS differences that were not shown graphically in the figure. When one removes the variance of the difference between the two Argo products from that between Aquarius and Argo, the resultant estimate, indicating the lower-bound of Aquarius SSS accuracy, is 0.04 psu for non-seasonal anomalies on 10°x10° scale. The latter is closer to the 0.03 psu STD value between the two Argo products.

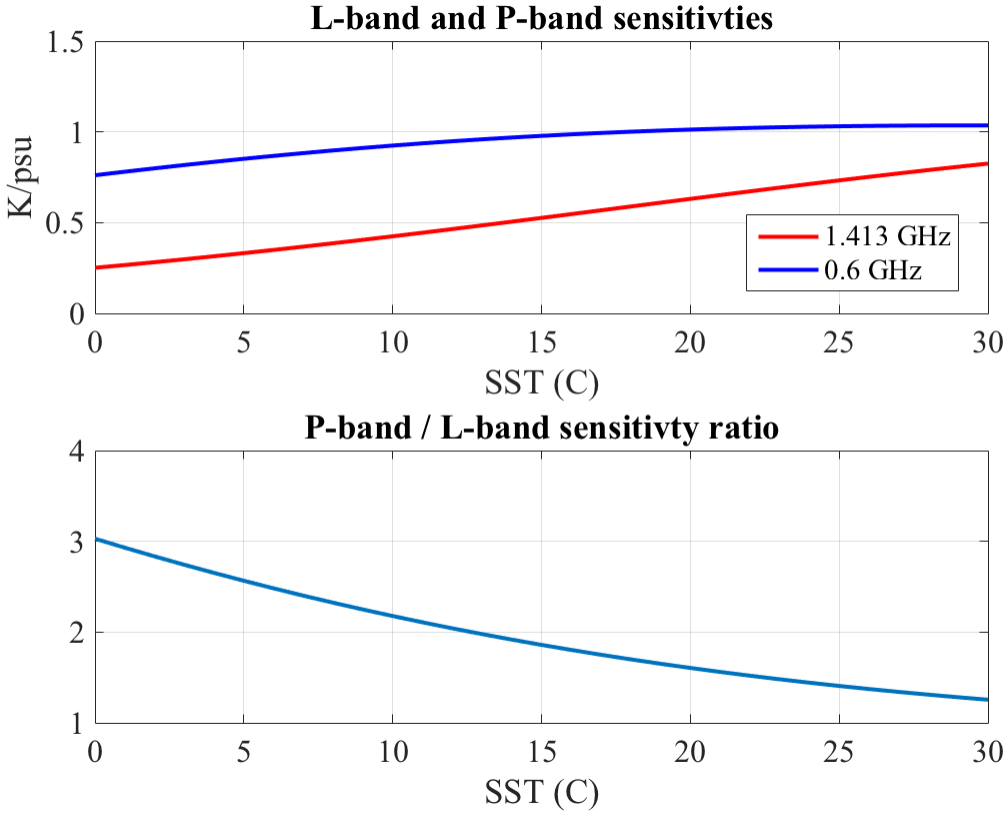

Figure 6. Sensitivity (K/psu) of ocean brightness temperature (T_B) to SSS as a function of SST for L-band (~1.4 GHz, red curve) and P-band (~0.6 GHz, blue curve) (upper), and the ratio of P-band/L-band sensitivity as a function of SST (lower). P-band has 2.6 to 3 times better sensitivity than L-band at SST range of 0-5°C.

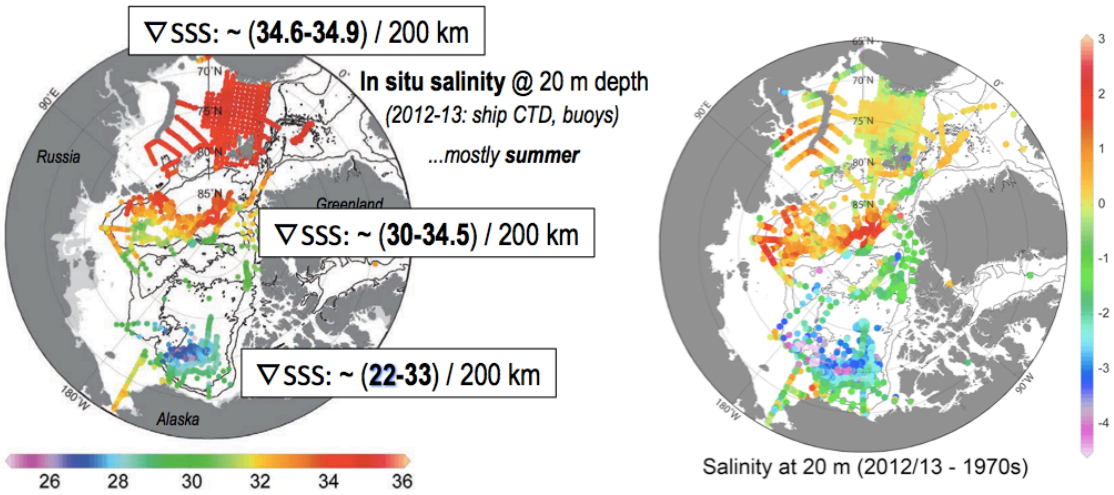

Figure 7. Left: spatial distribution of 20-m salinity based on in-situ measurements in the Arctic Ocean during 2013. Right: 20-m salinity difference between 2012/13 and 1970s climatology (based on Timmermans et al. 2014 and NOAA Arctic Report Card: 2013 Update http://www.arctic.noaa.gov/report13/ocean_temperature_salinity.html). The gradient estimates were provided by Mike Steele of Applied Physics Laboratory, University of Washington.

References

1. Lee et al. (2015). Linkage of the Water Cycle, Ocean Circulation, and Climate. Response to 2017-2027 NRC Decadal Survey in Earth Science and Applications from Space Initial Request for White Papers.

2. Talley, L.D. (2002). Salinity patterns in the ocean. In Encyclopedia of global change. Volume: the earth system: physical and chemical dimensions of global environmental change (eds MacCracken MC, Perry JS), pp. 629–640. Chichester, UK: John Wiley & Sons.

3. IPCC (2013). Climate Change 2013: The Physical Science Basis. Working Group 1 Contribution to the Fourth Assessment Report of the Intergovernmental Panel on Climate Change . Cambridge University Press, 1535 pp.

4. Chen, X-Y. and K.-K. Tung (2014). Varying planetary heat sink led to global-warming slowdown and acceleration. Science, 897-903 DOI: 10.1126/science.1254937.

5. Haine, W.N.T, B. Curry, and R. Gerdes et al. (2015). Arctic freshwater export: Status, mechanisms, and prospects. Global and Planetary Change. 125, 13-35. doi:10.1016/j.gloplacha.2014.11.013.

6. Gordon, A.L., (2014). Oceanography: Southern Ocean polynya, News and Views for Nature Climate Change, vol (4), 249–250; doi:10.1038/nclimate2179.

7. Newsom, E.R., C.M. Bitz, F.O. Bryan, R. Abernathey, P.R. Gent (2016). Southern Ocean deep circulation and heat uptake in a high-resolution climate model. J. Clim., 29, 2597-2619.

8. Holte, J. W., L. D. Talley, T. K. Chereskin, and B. M. Sloyan (2012). The role of air-sea fluxes in Subantarctic Mode Water formation, J. Geophys. Res., 117, C03040, doi:10.1029/2011JC007798.

9. Bourassa, M. A., S. T. Gille, C. Bitz, D. Carlson, C. A. Clayson, I. Cerovecki, M. F. Cronin, W. M. Drennan, C. W. Fairall, R. N. Hoffman, G. Magnusdottir, R. T. Pinker, I. A. Renfrew, M. Serreze, K. Speer, L. D. Talley, and G. A. Wick (2013). High-latitude ocean and sea ice surface fluxes: Challenges for climate research, *Bull. Amer. Met. Soc.*, 94, 403-423.

10. Lukas, R., and E. Lindstrom (1991). The Mixed Layer of the Western Equatorial Pacific-Ocean, Journal of Geophysical Research-Oceans, 96, 3343-3357.

11. Sprintall, J., and M. Tomczak (1992). Evidence of the barrier layer in the surface layer of the tropics, Journal of Geophysical Research- Oceans, 97 (C5), 7305-7316.

12. Ballabrera-Poy, J., R. Murtugudde, and A.J. Busalacchi et al. (2002). On the potential impact of sea surface salinity observations on ENSO predictions. J. Geophys. Res., 107, DOI: 10.1029/2001JC000834.

13. Hackert, E., Ballabrera-Poy, J., Busalacchi, A. J., Zhang, R. H., & Murtugudde, R. (2011). Impact of sea surface salinity assimilation on coupled forecasts in the tropical Pacific. Journal of Geophysical Research: Oceans (1978–2012), 116(C5).

14. Hackert, E., Busalacchi, A.J., and Ballabrera-Poy, J. (2014). Impact of Aquarius Sea Surface Salinity Observations on Coupled Forecasts for the Tropical Indo-Pacific Ocean, J. Geophys. Research. 119 (7), 4045-4067, doi:10.1002/2013JC009697.

15. Zhao, M. and co-authors (2013). Impact of Salinity Constraints on the Simulated Mean State and Variability in a Coupled Seasonal Forecast Model. Monthly Weather Review. 141, 388-402. DOI: 10.1175/MWR-D-11-00341.1

16. Zhu, J. and co-authors (2014). Salinity anomaly as a trigger for ENSO events. Nature. 4, No.6912. doi:10.1038/srep06821.

17. Zheng, F and R. Zhang (2015). Interannual varying salinity effects on ENSO in the tropical Pacific: a diagnostic analysis from Argo. Ocean Dyn., DOI: 10.1007/s10236-015-0829-7.

18. Schmitt, R.W. (1995). The ocean component of the global water cycle. Pp. 1,395 1,409 in US National Report to International Union of Geodesy and Geophysics, 1991 1994, Supplement to Reviews of Geophysics.

19. Trenberth, K. and co-authors (2007). Estimates of the global water budget and its annual cycle using observational and model data. J. Hydrometeor. 758-769. DOI: 10.1175/JHM600.1.

20. Schanze, J. J., Schmitt, R. W., & Yu, L. L. (2010). The global oceanic freshwater cycle: A state-of-the-art quantification. Journal of Marine Research, 68(3-4), 569-595.

21. Durack, P.J., S.E. Wijffels, R.J. Matear (2012). Ocean salinity reveal strong global water cycle intensification during 1950 to 2000. Science. 336, 455-458.

22. Schmitt, R.W. (2008). Salinity and the global water cycle. Oceanography 21(1):12–19.

23. Lagerloef, G., R. Schmitt, J. Schanze, and H.-Y. Kao (2010). The ocean and the global water cycle. Oceanography 23(4):82–93, doi:10.5670/oceanog.2010.07.

24. Helm, K. P., N. L. Bindoff and J. A. Church (2010) Changes in the global hydrological-cycle inferred from ocean salinity. Geophysical Research Letters, 37 (18), L18701. doi: 10.1029/2010GL044222.

25. Skliris, N., R. Marsh, S. A. Josey, S. A. Good, C. Liu, R. P. Allan (2014) Salinity changes in the World Ocean since 1950 in relation to changing surface freshwater fluxes. Climate Dynamics, 43 (3-4), pp 709-736. doi: 10.1007/s00382-014-2131-7.

26. Boyer, T.P., S. Levitus, J.I. Antonov, R.A. Locarnini, and H.E. Garcia (2005). Linear trends in salinity for the world ocean, 1955–1998. Geophysical Research Letters 32, L01604, doi:10.1029/2004GL021791.

27. Gordon, A., and C.F. Giulivi (2008). Sea surface salinity trends over 50 years within the subtropical North Atlantic. Oceanography 21(1): 20–29.

28. Lee, T. (2016). Consistency of Aquarius sea surface salinity with Argo products on various spatial and temporal scales. Geophys. Res. Lett., 10.1002/2016GL068822. Published online 28 April 2016.

29. Li, L., R.W. Schmitt, C.C. Ummenhofer, K. B. Karnauskas (2016a). North Atlantic Salinity as a Predictor of Sahel Rainfall. Science Advances. Vol. 2, No.5, DOI:10.1126/sciadv.1501588.

30. Li, L., R.W. Schmitt, C.C. Ummenhofer, K. B. Karnauskas (2016b). Implications of North Atlantic Sea Surface Salinity for Summer Precipitation over the US Midwest: Mechanisms and Predictive Value. J. Climate, In press. Early online release: http://journals.ametsoc.org/doi/pdf/10.1175/JCLI-D-15-0520.1

31. Doney, S., K. Lindsay, and K. Caldeira, et al. (2004). Evaluating global ocean carbon models: The importance of realistic physics. Global Biogeochemical Cycles.18. DOI: 10.1029/2003GB002150.

32. Williams, R.G. and M.J. Follows (2011). Ocean dynamics and the carbon cycle: Principles and mechanisms. Cambridge University Press. ISNB: 9780521843690.

33. Keeling, R. F. & Peng, T-H. Transport of heat, CO_2 and O_2 by the Atlantic's thermohaline circulation. Phil. Trans. R. Soc. Lond. B 348, 133–142 (1995); 348, 133–142 (1995).

34. Sabine, C. L. et al. (2004). The oceanic sink for anthropogenic CO_2. Science 305, 367–371.

35. Sarmiento, J. L., N. Gruber, and M. A. Brzezinski et al.(2004). High-latitude controls of thermocline nutrients and low latitude biological productivity. Nature. 427, 56-60. doi:10.1038/nature02127.

36. Landschützer P, Gruber N, Haumann FA, Rödenbeck C, Bakker DCE, van Heuven S, Hoppema M, Metzl N, Sweeney C, Takahashi T,Tilbrook, B. and Wanninkhof, R. (2015). The reinvigoration of the Southern Ocean carbon sink, Science, 349, 1221-1224. doi: 10.1126/science.aab2620).

37. Turk, D., C. J. Zappa, C. S. Meinen, J. R. Christian, D. T. Ho, A. G. Dickson, and W. R. McGillis (2010), Rain impacts on CO_2 exchange in the western equatorial Pacific Ocean, Geophys. Res. Lett., 37(23).

38. LEFÈVRE, N., DIVERRÈS, D. and GALLOIS, F. (2010), Origin of CO2 undersaturation in the western tropical Atlantic. Tellus B, 62: 595–607. doi: 10.1111/j.1600-0889.2010.00475.x

39. Lee, K., L.T. Tong, F. J. Millero, C.L. Sabine, A.G. Dickson, C. G. Geun-Ha Park, R. Wanninkhof, R. A. Feely, and R.M. Key (2006). Global relationships of total alkalinity with salinity and temperature in surface waters of the world's oceans. Geophysical Research Letters. 33, L19605, doi:10.1029/2006GL027207.

40. Sun, Q., D. Tang, and S. Wang (2012): Remote-sensing observations relevant to ocean acidification, International Journal of Remote Sensing, 33:23, 7542-7558.

41. Sabia R., D. Fernández-Prieto, J. Shutler, C. Donlon, P. Land, N. Reul, Remote sensing of surface ocean pH exploiting sea surface salinity satellite observations, Proceedings of IGARSS 2015 (International Geoscience and Remote Sensing Symposium), Milano, Italy, July 27 –31, 2015.

42. Salisbury, J., D. Vandemark, B. Jönsson, W. Balch, S. Chakraborty, S. Lohrenz, B. Chapron, B. Hales, A. Mannino, J.T. Mathis, N. Reul, S.R. Signorini, R. Wanninkhof, and K.K. Yates. (2015). How can present and future satellite missions support scientific studies that address ocean acidification? Oceanography 28(2):108–121

43. Land, P., J. Shutler, H. Findlay, F. Girard-Ardhuin, R. Sabia, N. Reul, J.-F. Piolle, B. Chapron, Y. Quilfen, J. Salisbury, D. Vandemark, R. Bellerby, and P. Bhadury (2015). Salinity from space unlocks satellite-based assessment of ocean acidification. Environmental Science & Technology, DOI: 10.1021/es504849s.

44. Brown, C. W., J. Boutin, and L. Merlivat (2016), New insights of pCO2 variability in the tropical eastern Pacific Ocean using SMOS SSS, Biogeosciences , in press.

45. Fine, R.A., D.A. Wiley, and F.J. Millero (2016). Global variability and changes in ocean total alkalinity from Aquarius satellite. Geophysical Research Letters. Submitted.

46. Thompson, A.F., A.L. Stewart and T. Bischoff (2016). A multi-basin residual-mean model for the global overturning circulation. J. Phys. Oceanogr., in revision.

47. Sloyan, B.M., and I.V. Kamenkovich (2007). Simulation of Subantarctic Mode and Antarctic Intermediate Waters in climate models. J. Climate., **20**, 5061-5080.

48. Huntington, T.G. (2006). Evidence for intensification of the global water cycle: review and synthesis. Journal of Hydrology. 319, 83-95. doi:10.1016/j.jhydrol.2005.07.003.

49. Hegerl, G. C., E. Black, R. P. Allan, et al. (2015). Challenges in quantifying changes in the global water cycle. Bulletin of the Meteorological Society, 96 (7), 1097-1115. doi: 10.1175/BAMS-D-13-00212.1.

50. Dai, A., T. Qian, K.E. Trenberth, and J.D. Milliman (2009). Changes in continental freshwater discharge from 1948 to 2004. Journal of Climate 22:2,773–2,792.

51. Josey, S. A., S. Gulev, and L. Yu (2013). Exchanges Through the Ocean Surface (Chapter 5). In: Ocean Circulation and Climate – A 21st Century Perspective (Second Edition), Siedler, G., S. M. Griffies, J. Gould and J. A. Church (Eds), Volume 103, pp 105-140, International Geophysics, Academic Press, Elsevier, Oxford OX5 1GB, UK. doi: 10.1016/B978-0-12-391851-2.00005-2.

52. Robertson, F. R., M. G. Bosilovich, J. B. Roberts, R. H. Reichle, R. Adler, L. Ricciardulli, W. Berg and G. J. Huffman (2014). Consistency of Estimated Global Water Cycle Variations over the Satellite Era. Journal of Climate, 27 (16), 6135-6154. doi: 10.1175/JCLI-D-13-00384.1.

53. Rawlins, M.A., M. Steele , M.C. Serreze , et al. (2009). Tracing freshwater anomalies through the air-land-ocean system: A case study from the Mackenzie river basin and the Beaufort Gyre. Atmosphere-Ocean, 47:1, 79-97, DOI:10.3137/OC301.2009.

54. Martin, A., Boutin, J., Hauser, D., Reverdin, G., Pard_e, M., Zribi, M., Fanise, P., Chanut, J., Lazure, P., Tenerelli, J., et al., (2012). Remote sensing of sea surface salinity from carols l-band radiometer in the gulf of biscay. Geoscience and Remote Sensing, IEEE Transactions on 50 (5), 1703{1715.

55. Fournier, S., T. Lee, and M. Gierach (2016). Seasonal and interannual variations of sea surface salinity associated with the Mississippi River plume observed by SMOS and Aquarius. Remote Sensing. Environ. 180, 431-439, http://dx.doi.org/10.1016/j.rse.2016.02.050 .

56. Cavalieri, D.J. and C. L. Parkinso (2012). Arctic sea ice variability and trends, 1979–2010. The Cryosphere. 6, 881–889. doi:10.5194/tc-6-881-2012.

57. Toole, J.M., R.A. Krsihfield, M.L. Timmermans, et al. (2011). The Ice-tethered profiler: Argo of the Arctic. Oceanography. 24(3):126–135. http://dx.doi.org/10.5670/oceanog.2011.64.

58. Terray, L., L. Corre, S. Cravatte, T. Delcroix, G. Reverdin, and A. Ribes (2011), Near-Surface Salinity as Nature's Rain Gauge to Detect Human Influence on the Tropical Water Cycle, Journal of Climate, 25(3), 958-977, doi:10.1175/jcli-d-10-05025.1.

59. Guan, B, T. Lee, D. Waliser, and D. Halkides, 2014: Aquarius Surface Salinity and the Madden-Julian Oscillation: the Role of Salinity in Surface Layer Density and Potential Energy. Geophys. Res. Lett., 41, doi:10.1002/2014GL059704.

60. Stammer, D., K. Ueyoshi, A. Köhl, W.B. Large, S. Josey, and C. Wunsch (2004). Estimating air-sea fluxes of heat, freshwater and momentum through global ocean data assimilation. Journal of Geophysical Research 109, C05023, doi:10.1029/2003JC002082.

61. Köhl, A., Sena Martins, M., & Stammer, D. (2014). Impact of assimilating surface salinity from SMOS on ocean circulation estimates. Journal of Geophysical Research: Oceans, 119(8), 5449-5464.

62. Vinogradova, N. R. Ponte, and I. Fukumori et al. (2014). Estimating satellite salinity errors for assimilation of Aquarius and SMOS data into climate models. J. Geophys. Res. 119, DOI: 10.1002/2014JC009906.

63. Toyoda, T., Y. Fujii, and T. Kuragano et al. (2015). Improvements to a global ocean data assimilation system through the incorporation of Aquarius surface salinity data. J. Geophys. Res. DOI: 10.1002/qj.2561.

64. Shao, A. E., S. T. Gille, S. Mecking, and L. Thompson (2015). Properties of the Subantarctic Front and Polar Front from the skewness of sea level anomaly, J. Geophys. Res. Oceans, 120, 5179–5193, doi:10.1002/2015JC010723.

65. Fore, A.G., Simon H. Yueh, Wenqing Tang, Bryan W. Stiles, and Akiko K. Hayashi, Combined Active / Passive Retrievals of Ocean Vector Wind and Sea Surface Salinity with SMAP, IEEE Trans. Geosci. Remote Sens. Under review, 2016.

66. Kaleschke, L., X. Tian-Kunze, N. Maaß, M. Mäkynen, and M. Drusch (2012), Sea ice thickness retrieval from SMOS brightness temperatures during the Arctic freeze-up period, Geophys. Res. Lett., doi:10.1029/2012GL050916.

67. Reul, N., S. Fournier, and J. Boutin et al. (2014). Sea Surface Salinity Observations from Space with the SMOS Satellite: A New Means to Monitor the Marine Branch of the Water Cycle, Surv Geophys, 35(3), 681-722, doi:10.1007/s10712-013-9244-0.

68. Lagerloef, G., A. deCharon, and E. Lindstrom (2013). Ocean salinity and the Aquarius/SAC-D mission: a new frontier in ocean remote sensing. Marine Tech. Soc. Journal. 47, 5, 26-30. DOI: http://dx.doi.org/10.4031/MTSJ.47.5.1.

69. Entekhabi, D., E. G. Njoku, P. E. O'Neill, K. H. Kellogg, W. T. Crow, W. N. Edelstein, J. K. Entin, S. D. Goodman, T. J. Jackson, J. Johnson, J. Kimball, J. R. Piepmeier, R. D. Koster, N. Martin, K. C. McDonald, M. Moghaddam, S. Moran, R. Reichle, J. C. Shi, M. W. Spencer, S. W. Thurman, L. Tsang, and J. Van Zyl, The Soil Moisture Active Passive (SMAP) Mission, Proceedings of IEEE, Vol. 98,No. 5,pp. 704-716, May 2010.

70. Yueh, S. H., W. Tang, A. Fore, A. Hayashi, Y. T. Song, and G. Lagerloef (2014),Aquarius geophysical model function and combined active passive algorithm for ocean surface salinity and wind retrieval, J. Geophys. Res. Oceans, 119, 5360–5379, doi:10.1002/2014JC009939.

71. Yueh, S. H., W. Tang, A. Fore, G. Neumann, A. Hayashi, A. Freedman, J. Chaubell, and G. Lagerloef (2013). L-band Passive and Active Microwave Geophysical Model Functions of Ocean Surface Winds and Applications to Aquarius Retrieval. IEEE Trans. Geoscience and Remtoe Sensing, 51 (9), 4619-4632, DOI: 10.1109/TGRS.2013.2266915.

72. Meissner, T., F. J. Wentz, and L. Ricciardulli (2014). The emission and scattering of L-band microwave radiation from rough ocean surfaces and wind speed measurements from the Aquarius sensor, J. Geophys. Rev., 119, doi: 10.1002/2014JC009837.

73. Wentz et al. (2015). Aquarius Salinity Retrieval Algorithm Theoretical Basis Document (ATBD). Remote Sensing Systems. Santa Rosa, CA. [Available online at http://podaac.jpl.nasa.gov/SeaSurfaceSalinity/Aquarius].

74. Lagerloef, G., H.-Y. Kao, and T. Meissner et al. (2015). Aquarius Salinity Validation Analysis; Data Version 4.0. ftp://podaac-ftp.jpl.nasa.gov/allData/aquarius/docs/v4/AQ-014-PS-0016_AquariusSalinityDataValidationAnalysis_DatasetVersion4.0and3.0.pdf.

75. Huntemann, M., G. Heygster, L. Kaleschke, T. Krumpen, M. Mäkynen, and M. Drusch (2014). Empirical sea ice thickness retrieval during the freeze-up period from SMOS high incident angle observations.*The Cryosphere* 8, p. 439-451, doi:10.5194/tc-8-439-2014.

76. Timmermans, M.L., S. Cole, and J. Toole (2012). Horizontal Density Structure and Restratification of the Arctic Ocean Surface Layer. J. Phys. Oceanogr., DOI: http://dx.doi.org/10.1175/JPO-D-11-0125.1.

77. Steele, M., W. Ermold, and Jinlun Zhang (2008). Arctic Ocean surface warming trends over the past 100 years. GEOPHYSICAL RESEARCH LETTERS, VOL. 35, L02614, doi:10.1029/2007GL031651.

78. Steele, M., *and* W. Ermold (*2015*). Salinity trends on the Siberian Shelves. GEOPHYSICAL RESEARCH LETTERS, VOL. 31, L24308, doi:10.1029/2004GL021302.

79. Rabe, B.,M. Karcher, F. Kauker, et al. (2014). Arctic Ocean basin liquid freshwater storage trend 1992–2012, Geophys. Res. Lett., 41, 961–968, doi:10.1002/2013GL058121.

80. Dong, S.-F., S.L. Garzoli, and M. Baringer (2009). An assessment of the seasonal mixed-layer salinity budget in the Southern Ocean. J. Geophys. Res. DOI:10.1029/2008JC005258.

81. Morrow, R and E. Kesternare (2014). Nineteen-year changes in surface salinity in the Southern Ocean south of Australia. J. Mar. Res. 129, 472–483.

82. Margulis S. (TBC), Wade Crow, Susan Steele-Dunne, Alexander Konings, Joel Johnson, Mahta Moghaddam, Binayak Mohanty, Sassan Saatchi, Bridget Scanlon, Russel Scott, Eric Small, Simon Yueh and Michael Spencer, Groundwater Recharge and Evapotranspiration: Fluxes at the Interface of Water, Energy, Biogeochemical and Human Systems, 2017 Decadal Survey Response, May 2016

83. Mahta Moghaddam, Scott Goetz, John Kimball, Randy Koster, Walter Oechel, Rolf Reichle, Sassan Saatch, Permafrost Active Layer Dynamics Represent a Critical Climate Feedback Requiring Space-based Measurements, 2017 Decadal survey response, May 2016.

84. Sassan Saatchi, James Randerson, John Kimball, Gabriel Katul, Ram Oren, Alexandra Konings, Dara Entekhabi, Mahta Moghaddam, David Schimel, Josh Fisher, and Simon Yueh, Ecosystem Vulnerability to Water Stress: Response of Global Carbon Cycle to Extreme Climate. 2017 Decadal survey response, May 2016.